Design of a graphene oxide-BODIPY conjugate for glutathione depletion and photodynamic therapy

Giacomo Reina, Amalia Ruiz, Barbara Richichi, Giacomo Biagiotti, Gina E Giacomazzo, Lucas Jacquemin, Yuta Nishina, Cécilia Ménard-Moyon, Wafa T Al-Jamal, Alberto Bianco

Design of a graphene oxide-BODIPY conjugate for glutathione depletion and photodynamic therapy

Giacomo Reina,[1,#,‡] Amalia Ruiz,[2,#] Barbara Richichi,[3,4] Giacomo Biagiotti,[3,4] Gina E. Giacomazzo,[3] Lucas Jacquemin,[1] Yuta Nishina,[5,6] Cécilia Ménard-Moyon,[1] Wafa T. Al-Jamal,[2,] Alberto Bianco[1],**

[1]CNRS, Immunology, Immunopathology and Therapeutic Chemistry, UPR 3572, University of Strasbourg, ISIS, 67000 Strasbourg, France.

[2]School of Pharmacy – Queen's University Belfast, Belfast, BT9 7BL, United Kingdom.

[3] Department of Chemistry 'Ugo Schiff', University of Firenze, Via della Lastruccia 13, 50019 Sesto Fiorentino (FI, Italy).

[4] Consorzio Interuniversitario Nazionale per la Scienza e Tecnologia dei Materiali (INSTM, Via G. Giusti, 9, 50121 Firenze (Italy).

[5]Graduate School of Natural Science and Technology, Okayama University, 3-1-1 Tsushima-naka, kita-ku, Okayama, 700-8530, Japan.

[6]Research Core for Interdisciplinary Sciences, Okayama University, 3-1-1 Tsushima-naka, kita-ku, Okayama, 700-8530, Japan.

Correspondance to: a.bianco@ibmc-cnrs.unistra.fr, w.al-jamal@qub.ac.uk

[#]These authors contributed equally to this work

[‡]Present address: Graduate School of Human and Environmental Studies, Kyoto University, Sakyo-ku, Kyoto 606-8501, Japan.

Keywords: Carbon materials; functionalisation; photosensitisers; reactive oxygen species; cancer therapy

Abstract

Boron dipyrromethene derivates (BODIPYs) are promising photosensitisers (PSs) for cancer treatment using photodynamic therapy (PDT). This study investigates the functionalisation of graphene oxide (GO) with a BODIPY derivate for glutathione (GSH) depletion and PDT. The functionalisation of GO with a 3,5-dichloro-8-(4-boronophenyl) BODIPY *via* a diol derivatisation with the phenyl boronic acid moiety at the *meso* position of the BODIPY core, allowed to preserve the intrinsic properties of GO. We demonstrated that both chlorine atoms were substituted by GSH in the presence of glutathione transferase (GST), inducing a relevant bathochromic shift in the absorption/emission features and thus generating the active PS. *Ex vitro* assessment using cell lysates containing cytoplasmatic GST revealed the intracellular catalytic mechanism for the nucleophilic substitution of the GO-BODIPY adduct with GSH. Confocal microscopy studies showed important differences in the cellular uptake of free BODIPY and GO-BODIPY and revealed the coexistence of GO-BODIPY, GO-BODIPY-GS, and GO-BODIPY-GS_2 species inside vesicles and in the cytoplasm of the cells after 24 h of incubation. *In vitro* biocompatibility and safety of GO and GO-BODIPY were evaluated in 2D and 3D models of prostate adenocarcinoma cells (PC-3), where no toxicity was observed up to 100 μg/mL of GO/GO-BODIPY in all treated groups 24 h post-treatment (cell viability > 90%). Only a slight decrease to 80% at 100 μg/mL was observed after 48 h of incubation. We demonstrated the efficacy of a GO adduct containing an α-chlorine-substituted BODIPY for the simultaneous depletion of intracellular GSH and the photogeneration of reactive oxygen species using a halogen white light source (5.4 mW/cm^2) with a maximum in the range of 500-800 nm, which significantly reduced cell viability (< 50%) after irradiation. Our study provides a new vision on how to apply BODIPY derivates and potentiate the toxicity of PDT in prostate and other types of cancer.

Introduction

Photodynamic therapy (PDT) has emerged as a promising therapeutic strategy for cancer treatment.[1] PDT is a spatially targeted minimally invasive technique that, due to its local activity, is associated with low side effects. Effective PDT requires three key components, namely a photosensitiser (PS), light and oxygen.[2] Compared to radiotherapy, chemotherapy and surgery, PDT may induce an immune response, thus making it compatible with cancer immunotherapy.[3] In recent years, new classes of PSs with higher photostability, greater ROS generation capacity and lower dark toxicity were designed.[4] Different molecules from this second generation of PSs have reached the clinical stage in cancer therapy. Metalloporphyrins, including Lutrin® and Lutex®, purpurins, like Purlytin®, chlorins, such as Foscan®, or dipyrromethenes, like TOOKAD®, among others have been evaluated for different types of cancer, showing a widespread use in the clinical practice.[5] The advantage of a minimally invasive treatment where the ablation of localised tumours eliminates the cancer and avoids the side effects of a radical therapy, has made them very attractive for the treatment of prostate cancer (Lutex® and TOOKAD®).[5]

In this context, boron dipyrromethene derivates (BODIPYs) have been widely investigated as PSs thanks to their favourable extinction coefficients, light to dark toxicity ratio, and potential use in PDT and as fluorescent probes in molecular imaging.[6–10] BODIPYs are prepared *via* easy chemical synthesis while their photophysical properties can be tuned *ad hoc* varying the substituents on the skeleton obtaining complexes with long lifetimes and high quantum yields.[6] More recently, BODIPYs were investigated for PDT, where they are administered as prodrugs to be activated intracellularly.[11] Switchable halogenated BODIPYs are amongst the most commonly studied.[12] More interestingly, BODIPYs have been functionalised with different substituents to enhance cell targeting. For instance, a bromo-substituted BODIPY was designed to target biotin receptor overexpressed on the membrane of cancer cells,[13] while BODIPY PSs where bromine was replaced by iodine resulted with a higher efficacy once activated by reactive oxygen species (ROS).[14] Another important application of halogenated BODIPYs is their *in situ* biosensing activity of molecules containing thiols.[15] In particular, α-chlorine-substituted BODIPYs can react with organic sulphurs, such as cysteine or glutathione (GSH), *via* an aromatic nucleophilic substitution reaction.[15] The derivatisation in the 3-position of BODIPYs shows distinct

spectroscopic differences. Whilst the 3-mercapto-substitution allows an intense bathochromic shift into the absorption and emission properties, the 3-amino substitution is, in general, less sensitive.[15]

The use of an α-chlorine-substituted BODIPY targeting GSH has never been reported for PDT. Due to this aspect, a 3,5-dichloro-BODIPY derivate with a functional phenyl boronic moiety at the *meso* position of the BODIPY core was explored in this work for the selective detection of GSH.[16] In the context of cancer therapy, GSH depletion is an efficient strategy adopted in combination with different types of cancer treatments, including radiotherapy and photothermal therapy.[17] Regarding PDT, the depletion of GSH weakens the natural defences that cancer cells have on ROS formation, thus enhancing the efficacy of PDT.[17]

To increase their biological efficacy, BODIPYs have been conjugated to a wide range of nanocarriers. Among others, graphene oxide (GO) has been extensively used for drug delivery.[18] GO has a high surface area and abundant oxygenated groups, providing the possibility for multiple functionalisation using covalent and noncovalent approaches. Moreover, GO displays good biocompatibility and capacity to cross biological barriers (e.g. the blood–brain barrier for the treatment of gliomas) or being internalised by cells.[18–21] To date, few GO-BODIPY adducts have been reported as efficient nanotools for PDT. For instance, polymers containing photochromic spiropyran and BODIPY were anchored to GO for the preparation of an *in vivo* multicolour pH-sensing device.[22] Using a similar strategy, a zwitterionic BODIPY polymer was attached to GO for the detection of cancer cells *via* pH-dependent fluorescence.[23] Nevertheless, in both studies, the functionalisation conditions led to GO reduction, thus diminishing the presence of oxygenated groups essential for orthogonal multifunctionalisation and high dispersibility in physiological conditions. In another study, a BODIPY containing Mn complexes was adsorbed onto the GO surface for ROS and oxygen generation upon light irradiation.[24] However, noncovalent approaches generally lack specificity and release control once the nanotools are dispersed in biofluids. In this work, we describe the preparation of a covalent GO-BODIPY adduct in mild conditions, preserving the intrinsic properties of GO for PDT. A 3,5-dichloro-8-(4-boronophenyl) BODIPY was easily anchored onto the GO surface, exploiting the diol derivatisation of the phenyl boronic acid moiety at the *meso* position of the BODIPY core.[16,25] By this strategy, we combined the photoswitchable ability of chloride-BODIPY

with the versatile chemistry of phenyl boronic acid BODIPY derivate to bind 1,2 diols present onto the GO surface.[16] Herein, we demonstrate the successful engineering BODIPY-GS_2 as a new class of PSs, where both chlorine atoms were substituted in cells by GSH in the presence of glutathione transferase (GST), inducing a relevant bathochromic shift in the absorption/emission features. We also describe the efficacy of GO-BODIPY in 2D and 3D prostate cancer cell models, where high levels of ROS were generated upon light irradiation, resulting in significant cell death.

Results and discussion

GO-BODIPY synthesis and characterisation

Boronate esters have emerged as one of the most researched functional moieties for biomedical applications thanks to their behaviour as pH- and ROS-responsive functional groups.[26] They can be used as cleavable linkers onto the GO surface.[27] This strategy was used for doxorubicin delivery in cancer cells.[28] In this work, we have designed a new adduct between GO and BODIPY for activatable PS release and safer in situ PDT. For this purpose, GO with a size distribution centred at 430 nm (Fig. S1) was prepared according to the Nishina's reported method.[29] A phenylboronic acid dichloro-substituted BODIPY derivate,[16] named BODIPY in this work, was used as prodrug PS. The BODIPY was grafted onto the GO surface *via* diol derivatisation with the phenyl boronic acid moiety in water in mild conditions (Scheme 1).

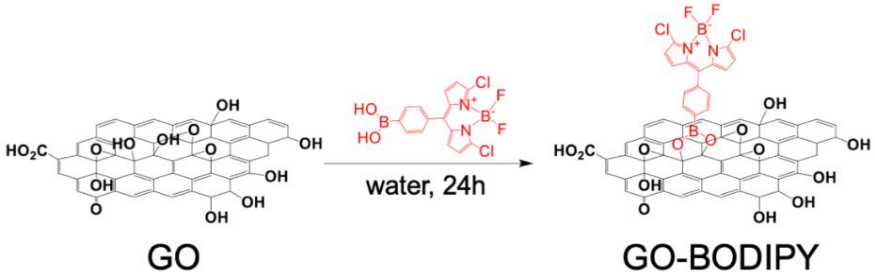

Scheme 1. Reaction of GO with BODIPY through diol derivatisation.[16] For the sake of clarity, the reaction is shown only on one diol moiety.

GO-BODIPY was characterised using different techniques, including SEM (Fig. S1) DLS, Z-potential (Table S1) thermogravimetric analysis (TGA), X-ray photoelectron microscopy

(XPS), UV-Vis and fluorescence spectroscopy. As reported in Table S1, the hydrodynamic size and Z-potential did not significantly change after the conjugation reaction. The functionalisation with BODIPY does not induce evident agglomeration or affect the colloidal stability of the material. The thermal profile of GO in inert atmosphere shows the typical two-step degradation profile with a first small step at around 100 °C and a second one at about 200 °C associated to water and labile oxygenated functions, respectively (Fig. S2).[30] BODIPY starts to degrade at about 100 °C and reaches a quasi-plateau after 400 °C. The GO-BODIPY degradation profile shows a weight loss at about 200 °C and a quasi-plateau at temperatures higher than 200 °C, showing the combined profiles of GO and BODIPY. The weight loss difference at 800 °C between GO and GO-BODIPY is an indication of the successful conjugation of the molecule onto the GO surface. XPS revealed the presence of fluorine, nitrogen, chlorine and boron onto the GO-BODIPY surface confirming the successful derivatisation (Fig. S3). We have taken into account F1s for the quantification of the amount of BODIPY onto GO due to the high photoemission cross-section of the F1s orbital.[31,32] From the XPS atomic percentage of F1s we could estimate a loading of 200 µmol of BODIPY per gram of material. Comparing this value with other functionalisation strategies, the diol esterification is as efficient as the approach based on epoxide opening, while it leads to a higher functionalisation degree compared to the derivatisation of the hydroxyls by esterification (about 100 µmol/g) or the Williamson reaction (about 30 µmol/g).[33,34] The photophysical characterisation of GO and GO-BODIPY is reported in Figure 1. The UV-Vis spectrum of BODIPY shows an absorption peak with a maximum at 512 nm induced by the chlorine substituent in 3 and 5 positions and associated to the π-π^* transition (Fig. 1 a).[16,35] The UV-Vis spectrum of GO is characterised by a typical broad signal monotonically decreasing assigned to the $n \rightarrow \pi^*$ transitions of the C=O bonds.[36] In the case of GO-BODIPY, the UV-Vis spectrum shows the presence of both BODIPY and GO adsorption bands. Interestingly, the absorption of BODIPY in the GO-BODIPY material is broadened, compared to that of the free BODIPY, which corroborates not only the conjugation of the chromophore onto GO, but also electronic interactions between the two species in the ground state.[37] The latter effect was already observed with other dyes covalently linked to GO surface.[38]

The characterisation of BODIPY and GO-BODIPY by fluorescence spectroscopy is reported in Fig. 1b and c, respectively. The BODIPY shows an emission peak centred at 525 nm.[16] The GO-BODIPY fluorescence shows similar results to the free BODIPY without any evident shifts, according with previously reported data on BODIPY conjugations,[39] but with a significant reduction in the fluorescence intensity. This observation can be ascribed to the quenching induced by GO near the BODIPY molecules. Such an effect was already described for GO in contact with different types of fluorophores.[19,40] While the mean BODIPY fluorescence lifetime was estimated 1.79 ns, the conjugation to GO induced a significant decrease in the BODIPY lifetime (Fig. 1d). The decay was fitted by a biexponential composed of a long lifetime (1.91 ns, 35%) and a short one (0.07 ns, 65%). This reduction can be attributed to the close proximity between the BODIPY and GO, resulting in an electron transfer and/or energy transfer between the fluorophore and the 2D material.[41]

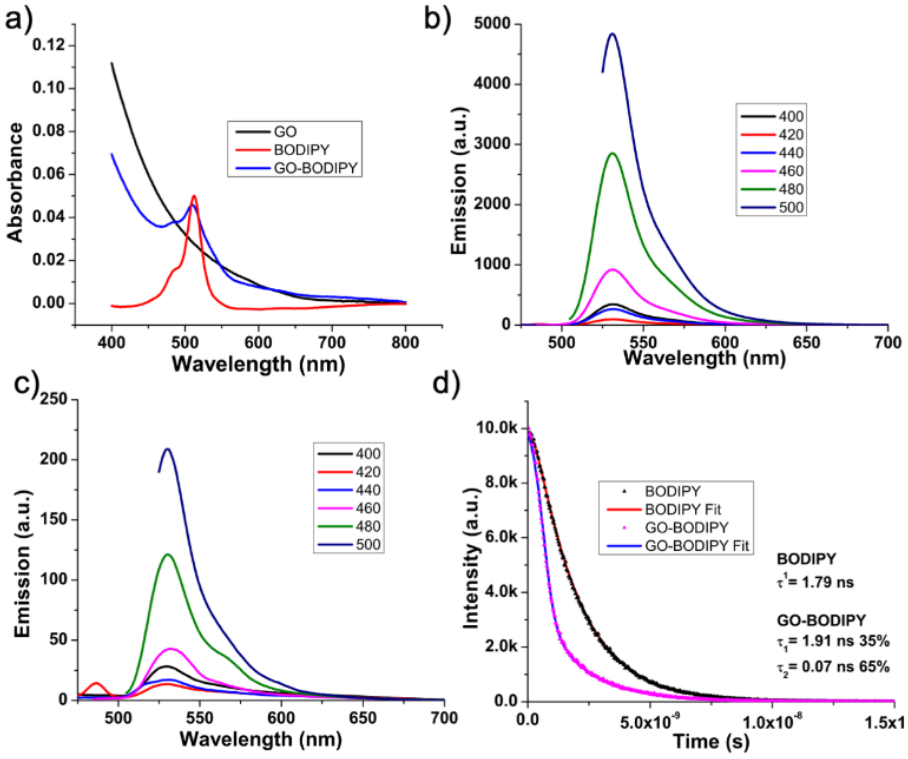

Figure 1. Photophysical characterisation of BODIPY and GO-BODIPY. a) UV-Vis spectra of GO (black line), BODIPY (red line) and GO-BODIPY (blue line). b) Fluorescence emission recorded from BODIPY at different excitation wavelengths. c) Fluorescence

emission recorded from GO-BODIPY at different excitation wavelengths. d) Lifetime of the excited state (λex = 495 nm, λem 523 nm) of BODIPY (black triangles) and its fitting (red line), GO-BODIPY (pink triangles) and its fitting (blue line); right: calculated lifetimes. All the solutions were freshly prepared at 5 μM of BODIPY (1:10, DMSO:water v/v), 20 μg/mL of GO (water) and 20 μg/mL (corresponding to 5 μM of BODIPY) of GO-BODIPY (water).

Nucleophilic substitution of chlorine with GSH

Taking into consideration the potential application of 3,5-dichlorine-substituted BODIPYs for the detection of molecules containing thiols,[42] we tested the ability of our GO-BODIPY conjugate to react with GSH (Fig. 2a). For this set of experiments, we simulated the intracellular conditions using a concentration of 10 mM of GSH.[43] UV-Vis spectroscopy shows that after 5 min incubation with GSH there is a clear bathochromic shift of the absorbance maximum (540 nm) accompanied with a hyperchromic effect (Fig. 2b). This behaviour can be associated to the mono-chlorine substitution by GSH, as described for other BODIPY structures (Fig. 2a, BODIPY-GS).[15] Interestingly, when the same reaction was performed in the presence of glutathione transferase, a further shift to 570 nm was recorded, again with a marked hyperchromic effect. GST is a detoxifying enzyme that protects cells from potentially harmful molecules and catalyses their conjugation with GSH,[44] showing a marked reactivity for halogenated compounds.[45] In our case, the extra bathochromic shift of the maximum of absorbance can be associated to the double substitution reaction of the chlorine substituents of BODIPY catalysed by GST (BODIPY-GS_2). This reaction was characterised by fluorescence spectroscopy (Fig. 2c). For this set of experiments, we recorded the spectra using two excitation wavelengths: 488 nm for the excitation of BODIPY and 560 nm for the excitation of BODIPY-GS_2. After incubation with GSH, the maximum of the emission spectra of BODIPY was recorded at 530 nm, when excited at 488 nm, as in the case for free BODIPY (Fig. 2c left). In contrast, at λ_{ex} = 560 nm only a small signal was recorded, due to the low absorbance of the BODIPY-GS at this wavelength. When GST was present, the emission profile totally changed (Fig. 2c right). Indeed, at λ_{ex} = 488 nm the fluorescence sensibly decreased, while at λ_{ex} = 560 nm a new emission peak appeared, with a maximum recorded at 580 nm. This shift in the

emission peak can be associated with the formation of BODIPY-GS2 catalysed by GST, accordingly with our previous data on chlorine mono- and bi-substitution reactions.[16] These changes in the emission properties of BODIPY can be also visualized in the Supporting Video 1 recorded under a UV lamp. The control solutions of BODIPY (5 µM) and BODIPY mixed with GSH (5 µM and 10 mM, respectively) displayed a stable green fluorescence. Upon addition of GST to the mixture of BODIPY and GSH, the emission of the solution turned to red within 5 min because of BODIPY-GS_2 formation.

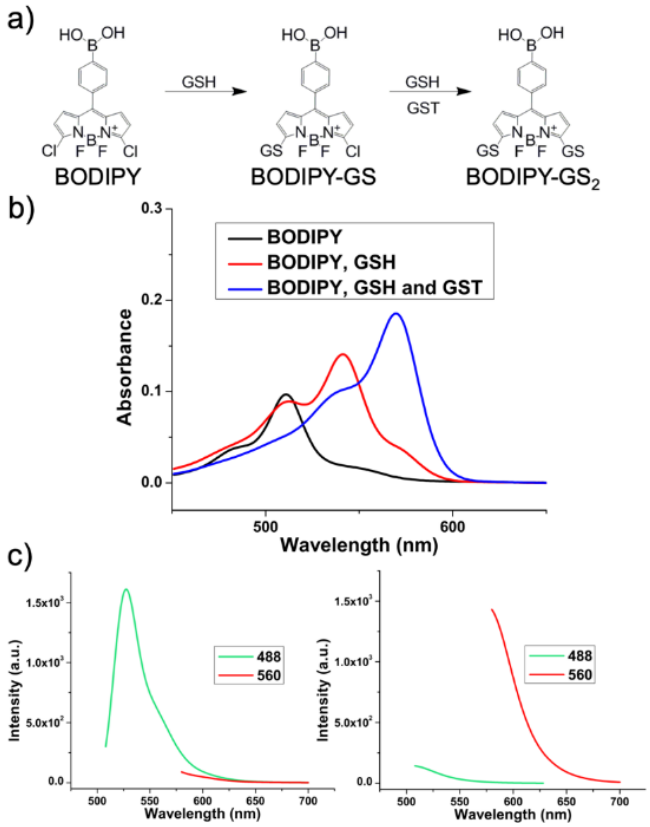

Figure 2. Reaction of BODIPY with GSH and GST. a) Nucleophilic substitution of chlorine with GST producing the mono and disubstituted BODIPY derivates. b): UV-Vis spectra of BODIPY (black line), BODIPY after 5 min incubation with GSH (red line), and BODIPY after 5 min incubation with GSH and GST. c) Fluorescence spectra of BODIPY incubated with GSH (left) and GSH in the presence of GST (right). Concentrations: 5 µM of BODIPY, 10 mM of GSH and 1.3 µM of GST. BODIPY was dissolved in DMSO/PBS (1:10 v/v).

We further investigated the reaction of BODIPY-GS_2 with cells. In this case, we lysed HeLa cells and extracted the cytoplasm. Subsequently, we incubated BODIPY or GO-BODIPY, and characterised the solutions/suspensions using UV-Vis and fluorescence spectroscopy (Fig. 3). Compared to water, the UV-Vis spectra of the solution of BODIPY in the lysate shows a lower absorption at 512 nm together with the appearance of two bands at 540 and 570 nm (Fig. 3a). This change can be explained by the incomplete reaction of BODIPY with GSH, leading to a mixture of unreacted BODIPY, BODIPY-GS, and BODIPY-GS_2. The fluorescence emission profile was also changed. Indeed, the solution of BODIPY in water shows a maximum emission peak at 525 nm when excited at 488 nm, while no significant emission was recorded using 560 nm excitation (Fig. 3b). Instead, in the extracted cell culture media, at λ_{ex} = 488 nm two emission bands were observed at 525 and 558 nm associated to BODIPY and BODIPY-GS, respectively (Fig. 3c). When excited at 560 nm, there was a strong emission band at 580 nm, associated to BODIPY-GS_2. Similar to free BODIPY, when GO-BODIPY was dispersed in cell extracts, a clear bathochromic shift of the absorbance was observed with new bands at 540 and 570 nm, associated to the reaction with GSH (Fig. 3d). The fluorescence profile of GO-BODIPY showed a comparative trend with free BODIPY (Fig. 3e and f). This behaviour confirms that the linkage of BODIPY to GO does not alter its reactivity with GSH molecules.

We investigated then the selectivity of the formation of BODIPY-GS_2 in different conditions. For this purpose, we calculated the ratio between the fluorescence intensity at 580 nm under λ_{ex} = 560 nm over the intensity at 525 nm under λ_{ex} = 488 nm (Fig. S4). This ratio corresponds to the ratio of BODIPY-GS_2 over free BODIPY.[42] As expected, for BODIPY in water the ratio was far below 0.1. When BODIPY was incubated with GSH, there was a negligible increase to 0.05, because GSH alone was able to generate only the mono-substituted BODIPY-GS (Fig. 2). When BODIPY was incubated with GSH and GST, the intensity ratio dramatically increased to almost 15. This is congruent with our previous observations, in particular with the UV-Vis spectra (Fig. 2b) where we observed a bathochromic shift associated to the formation of BODIPY-GS_2. We also tested cysteine, as it is an analyte that may compete with GSH. However, a negligible emission ratio (below 0.2) was recorded. Finally, when BODIPY was dispersed in HeLa cell lysate, a positive fluorescence intensity ratio higher than 4 was detected. This observation is in agreement

with the characterisation by UV-Vis and fluorescence spectroscopy (Fig. 3). GO-BODIPY was also tested in DMEM cell culture media and in HeLa cell lysate, giving similar results to free BODIPY. From our observations, the formation of BODIPY-GS_2 is catalysed by the GST enzyme. Indeed, free GSH neither in water nor in DMEM was unable to form BODIPY-GS_2.

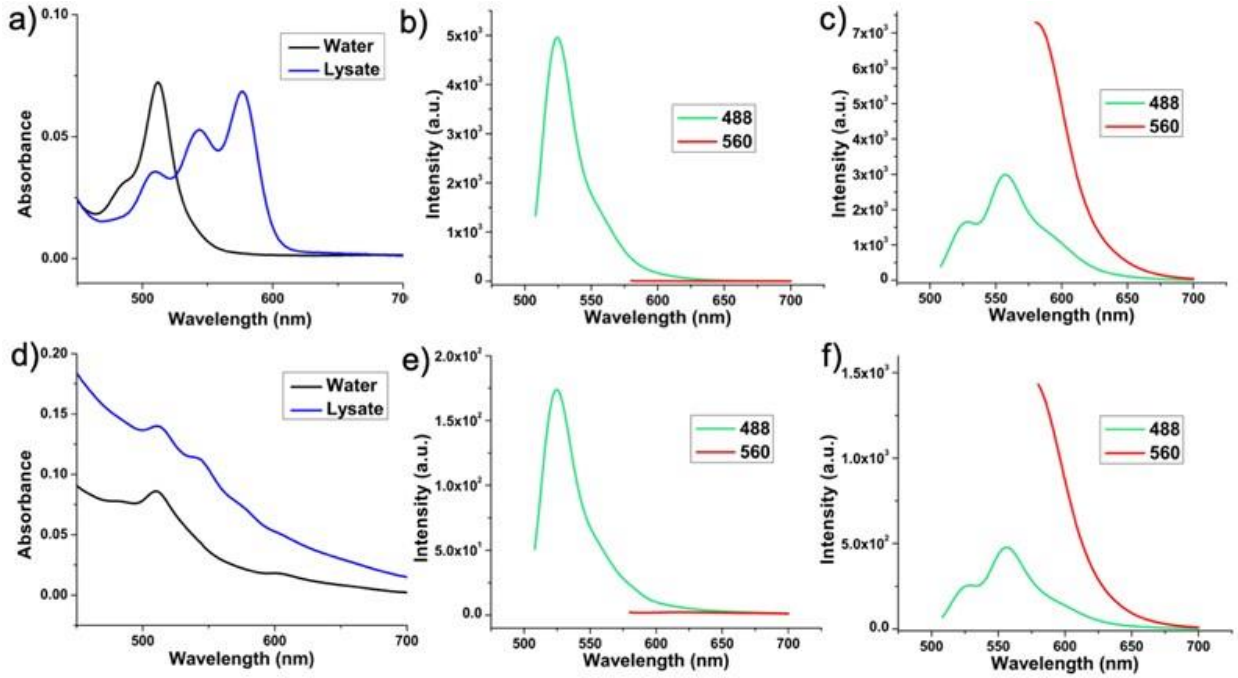

Figure 3. UV-Vis and fluorescence emission spectra of BODIPY and GO-BODIPY in water and in HeLa cell lysate. a) UV-Vis spectra of 5 µM BODIPY in water (black) and cell lysate (blue). b) Fluorescence emission spectra of 5 µM BODIPY in water excited at 488 nm (green) and at 560 nm (red). c) Fluorescence emission spectra of 5 µM BODIPY in HeLa cell lysate excited at 488 nm (green) and at 560 nm (red). d) UV-Vis spectra of 20 µg/mL GO-BODIPY in water (black) and cell lysate (blue). e) Fluorescence emission spectra of 20 µg/mL GO-BODIPY in water excited at 488 nm (green) and at 560 nm (red). f) Fluorescence emission spectra of 20 µg/mL GO-BODIPY in HeLa cell lysate excited at 488 nm (green) and at 560 nm (red).

Intracellular fate of BODIPY and GO-BODIPY

We tested the stability of GO-BODIPY incubated in DMEM for 24 h at 37 °C and filtered the suspension to see if any BODIPY was released in the media due to a potential boronic

ester hydrolysis (Fig. S5). No free BODIPY was detected, suggesting that the boronic ester bond was stable in cell culture media. Next, we investigated the internalisation of BODIPY and GO-BODIPY in HeLa cells by confocal microscopy (Fig. 4 and S5). The cells incubated with BODIPY or GO-BODIPY were observed at four different time points (0, 4, 8, and 24 h) by imaging BODIPY ($\lambda_{ex.}$ 488 nm, green signal) and BODIPY-GS_2 (λ_{ex} 560 nm, red signal). The free BODIPY immediately entered the cells and the fluorophore was converted into BODIPY-GS_2 (Fig. S6). The red staining was persistent and seemed to be diffused in most of the cell compartments up to 8 h. At 24 h, BODIPY-GS_2 was still present, mainly in cell vesicles. The cellular uptake kinetic of BODIPY conjugated onto GO sensibly changed (Fig. 4). Indeed, no fluorescence signal was recorded at time 0 and 4h, while few red and green dots were imaged after 8 h incubation. After 24 h, both green and red signals associated to GO-BODIPY and GO-BODIPY-GS_2, respectively, were more intense. In a previous study, we demonstrated that a similar batch of GO was internalised by HeLa cells in the timeframe interval between 8 and 24 h.[19] Thus, we can expect a similar uptake kinetic with GO-BODIPY. As also observed in HeLa cell lysate (Fig. 3), GO-BODIPY did not completely react with GSH, resulting in the coexistence of GO-BODIPY, GO-BODIPY-GS, and GO-BODIPY-GS_2. The red signal of GO-BODIPY-GS_2 seems to be located inside vesicles and in the cytoplasm of the HeLa cells. In contrast, the green signal associated to GO-BODIPY was much more diffused both after 8 and 24 h incubation. This dual localisation in the cytoplasm and vesicles agrees with the distribution of GST in the cells. GST can be localised soluble in the cytoplasm and in subcellular organelles like mitochondria, the endoplasmic reticulum, nucleus and the plasma membrane.[46,47] Furthermore, GST has been identified in peroxisomes which are membrane-bound organelle found in the cytoplasm of eukaryotic cells.[46] How glutathione is imported into peroxisomes is not clear yet. It has been suggested that the peroxisomal membrane is permeable to small metabolites; therefore, cytosolic glutathione is presumably delivered to the peroxisome lumen by diffusing across the peroxisomal membrane[48] and being available for GO-BODIPY-GS_2 formation.

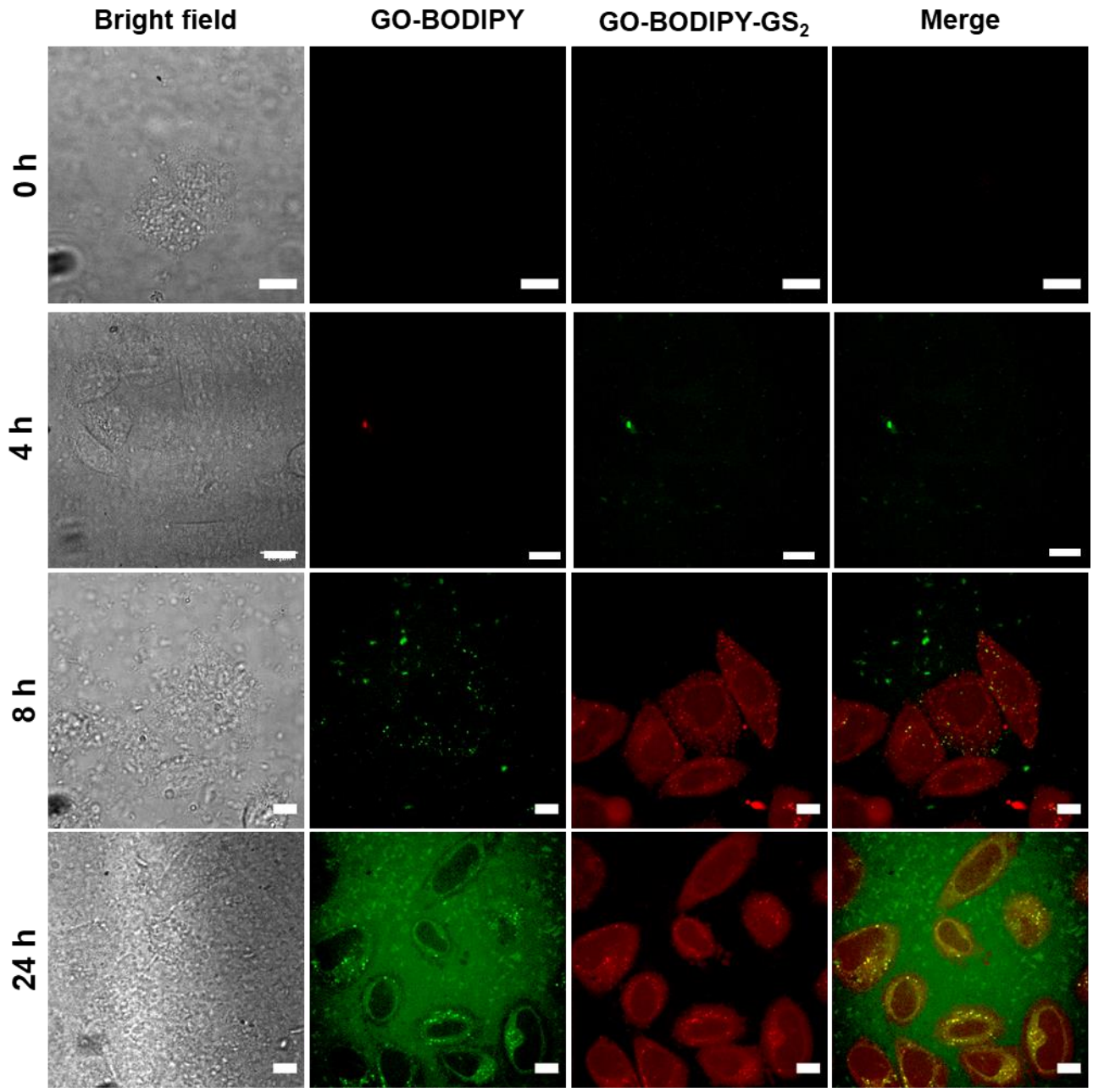

Figure 4. Live imaging of HeLa cells incubated with GO-BODIPY. HeLa cells were seeded overnight on 8-well chamber slide (Thermo Scientific) approximately 1×10^4 cells/cm^2, 500 µL/well. Next day, the cells were incubated with 20 µg/mL of GO-BODIPY and imaged at selected time points (rows). Green: GO-BODIPY, red: GO-BODIPY-GS_2. Scale bar: 10 µm.

***In vitro* cytotoxicity**

PDT is a promising strategy in delivering focal treatment in prostate cancer. For this reason, we evaluated the biocompatibility and safety of the materials by measuring the dark toxicity of GO or GO-BODIPY *in vitro* using the LDH assay in 2D and 3D models of prostate cancer (Fig. 5). Monolayers of prostate adenocarcinoma cells (PC-3) were treated with GO or GO-BODIPY up to 48 h with concentrations between 10 and 100 μg/mL of GO (Fig. 5a). No toxicity was observed in all treated groups 24 h post-treatment. However, a slight decrease in cell viability was obtained after 48 h for cells treated with control GO at 100 μg/mL (83.4%) relative to untreated cells. In the case of GO-BODIPY, we observed at 48 h some dose-dependent dark toxicity, with cell viability values ranging from 90% at 10 μg/mL to 80% at 100 μg/mL. These data are in agreement with other studies where cell viability decreased by 20% after exposure to GO concentrations around 10 μg/mL during 24 h or longer.[19,49]

Three-dimensional spheroids are promising models to evaluate the safety and therapeutic efficacy of new materials at a preclinical stage. The ability of spheroids to produce a higher order cellular organisation, and the potential to evaluate architectural factors influencing the penetration of the nanomaterials and the role of biochemical elements in the tumour (i.e., hypoxic core) offer great advantages. To better understand the behaviour of GO and GO-BODIPY in a tumour-like model, the toxicity of the materials was evaluated using a PC-3 spheroid model (Fig. 5b). The concentration of GO in the media was increased up to 200 μg/mL with an exposure time of 24 h. Interestingly, cell viability was always above 90% even at the highest concentration of both materials. Compared with the 2D model, the toxicity of both GO-based materials decreased. These results are in agreement with other studies where 3D models showed higher cell viability than the corresponding 2D systems, which could be attributed to lower cell-graphene interactions hindered by the limited diffusion of graphene sheets in the tumour model.[50]

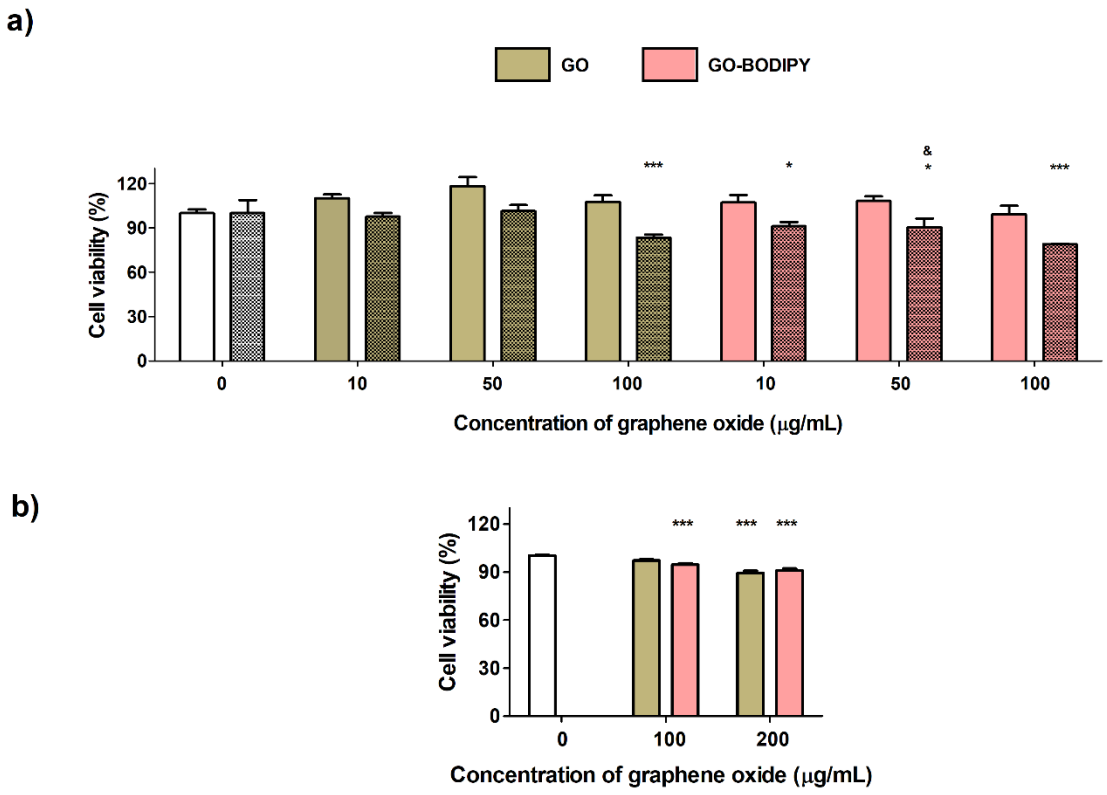

Figure 5. *In vitro* cytotoxicity of GO and GO-BODIPY. a) PC-3 monolayers (2×10^4/well) were seeded overnight in a 96 well-plate. Then, the cells were treated with GO or GO-BODIPY at different concentrations for 24 (solid bars) or 48 h (dotted bars). Cell viability was assessed *via* LDH assay. The results are expressed as average ± SD (n=4). Statistical analysis was performed using two-way ANOVA followed by Bonferroni post-test. * denotes comparison regarding the control (* $p<0.05$, ** $p<0.01$, *** $p<0.001$) and & denotes comparison between GO and GO-BODIPY (& $p<0.05$). b) PC-3 spheroids (5×10^3/well) were seeded in 1% agarose-coated 96 well-plates. Spheroids were incubated with the treatment 5 days after seeding when they reached a size of ~600 μm. Spheroids were treated with GO or GO-BODIPY at different concentrations for 24 h. Cell viability was assessed *via* LDH assay. The results are expressed as average ± SD (n=8). Statistical analysis was performed using two-way ANOVA followed by Bonferroni post-test. * denotes comparison regarding the control (*** $p<0.001$).

Photogeneration of reactive oxygen species

To further investigate the potential of GO-BODIPY for PDT in prostate cancer, the ROS generation capacity was evaluated using the permeable probe 2′-7′-dichlorodihydrofluorescein diacetate (DCFH-DA). DCFH-DA was incubated in both 2D and 3D PC-3 models before photoirradiation. This nonfluorescent molecule accumulates intracellularly, and subsequent oxidation yields the highly fluorescent product 2',7'-dichlorofluorescein that can be measured by an increase in fluorescence (λ_{exc} 485 nm, λ_{em} 535 nm). Fluorescence at 535 nm can be measured using a fluorescence multi-detection reader and was assumed to be proportional to the concentration of ROS in the cells after treatment with the nanomaterials.[51] The advantage of using a plate reader is that we are able to measure relative changes in the fluorescence of the cells *in situ* without the need for trypsinization or cell scraping, processes that themselves generate cellular oxidative stress and result in changes in fluorescence.[52]

PC-3 monolayers were incubated with 50 µg/mL for 24 h where no dark toxicity was observed before. Next day, the cells were incubated with DCFH-DA (10 µM, 1 h) to evaluate the ability of GO and GO-BODIPY to induce ROS generation. Then, the cells were washed twice with PBS and the light treatment was applied (150×10^3 J/m^2, 48 min). Figure 6a, corresponding to the treatment in monolayers, shows that both materials, GO and GO-BODIPY, induced a significant increase in ROS production compared with the control and non-irradiated samples. Remarkably, GO-BODIPY exhibited a higher capacity to induce ROS generation compared to GO alone. A 9.5-fold increase in the fluorescence was observed after photoirradiation of the cells treated with GO-BODIPY *vs* 3.9-fold change obtained for GO. The treatment with GO can cause an inflammatory response that produces relatively large amounts of free radicals.[2] It has been described in the literature that the increase in ROS level at GO concentrations as low as 4 µg/mL after 24 h incubation in HepG2 cells was due to a decrease in the mitochondrial membrane potential and the dysregulation of mitochondrial calcium equilibrium.[53] In addition, our functionalised material, GO-BODIPY, depleted the intracellular GSH, thus reducing the ROS scavenging capacity *via* GST, which contributes to an increased cell death. BODIPY molecules are a type II photosensitisers able to generate high quantity of singlet oxygen molecules through energy transfer mechanism.[54] However, in our experimental setup the presence of GSH, a

powerful scavenger, involved in the intracellular conjugation of the BODIPY-GS_2 would strongly interfere with the detection of the radical formed. The development of more robust methods for measuring ROS species and their reaction products in cells are needed.

When using PC-3 spheroids, we observed a significant reduction in the fluorescence compared with the monolayers (Fig. 6b). This could be caused by different factors, including a limited penetration of the 2D material in the spheroid model compared with the monolayer. Besides, for live cell fluorescence detection assays, the diffusion of fluorescent probes and penetration of photons for probe excitation and fluorescence emission must be considered comparing 2D and 3D models.[55] In this case, only a significant increase in ROS production was detected for cells treated with GO-BODIPY (1.2-fold increase).

These experiments highlight two important facts. The first one is the confirmation of intracellular ROS generation by GO and GO-BODIPY after the light treatment, most probably due to a mitochondrial damage, which is a common feature of the mechanism of toxicity of carbon-based nanomaterials with an enhanced ROS generation capacity by the latter due to the functionalisation with BODIPY.[51] The second fact is that we can observe how architectural factors influence the penetration and diffusion of the materials in 2D and 3D models and, in consequence, their ability to intracellularly generate ROS.

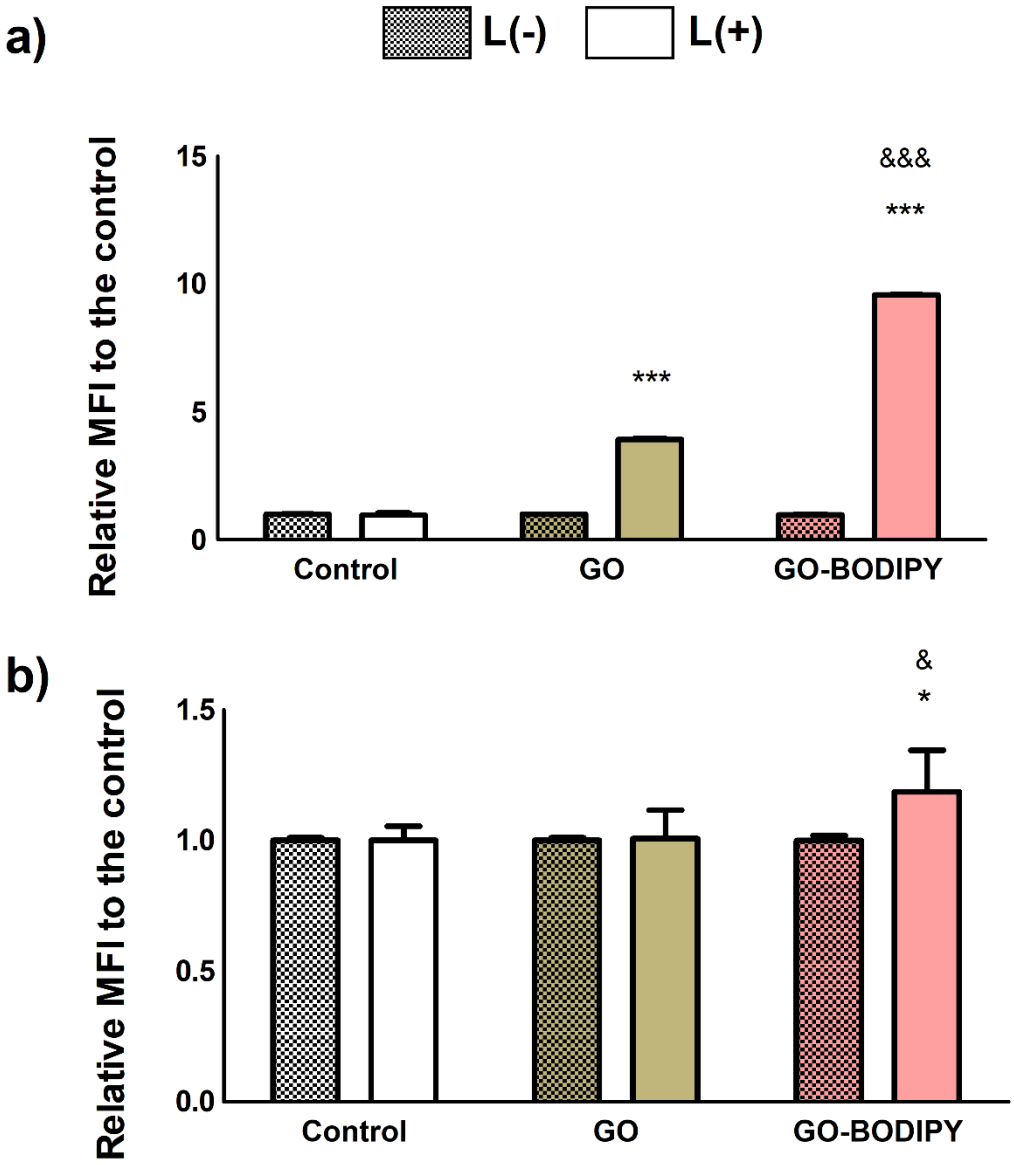

Figure 6. ROS production following GO and GO-BODIPY photoirradiation. a) PC-3 monolayers (2×10^4/well) were seeded overnight in a 96 well-plate. Then, the cells were incubated with GO or GO-BODIPY at 50 µg/mL for 24 h. Next day, the cells were incubated with 2′,7′-dichlorofluorescein (10 µM, 1 h). Then, the cells were washed twice with PBS and irradiated with light (150×10^3 J/m^2, 48 min) (solid bars), or kept non-irradiated (dotted bars). The fluorescence was measured before and after the PDT treatment (λ_{ex} = 485 nm, λ_{em} = 535 nm). The results are expressed as average ± SD (n=4). Statistical analysis was performed using one-way ANOVA followed by Bonferroni post-test. *

denotes comparison regarding the control (* $p<0.05$, ** $p<0.01$, *** $p<0.001$) and & denotes comparison between GO and GO-BODIPY (& $p<0.05$). b) PC-3 spheroids (5×10^3 /well) were seeded in 1% agarose coated 96 well-plates. The spheroids were incubated with GO or GO-BODIPY at 50 µg/mL for 24 h, 5 days after seeding when they reached a size of ~600 µm. Next day, the spheroids were incubated with DCFH-DA (10 µM, 1 h). Then, the spheroids were gently washed with PBS and irradiated with light (150×10^3 J/m^2, 48 min). After the treatment, the spheroids were incubated with a lysis solution (SDS 1%) for 30 min and then the media was transferred to a 96 well-plate. The fluorescence was measured at λ_{ex} = 485 nm, λ_{em} = 535 nm. The results are expressed as average ± SD (n=8). Statistical analysis was performed using one-way ANOVA followed by Bonferroni post-test. * denotes comparison regarding the control (* $p<0.05$) and & denotes comparison between GO and GO-BODIPY (& $p<0.05$).

Photodynamic efficacy

Having confirmed the capacity of GO-BODIPY to form BODIPY-GS2 intracellularly, catalysed by the GST enzyme, and the increased capacity of GO-BODIPY to generate ROS after photoirradiation, we investigated the potential of the conjugate as a PS for PDT. A successful PS requires exhibiting a low dark cytotoxicity, but an excellent toxicity when exposed to light. *In vitro* cytotoxicity after photoirradiation was measured by LDH assay in PC-3 monolayers and spheroids (Fig. 7). No toxicity was observed with cells irradiated in the absence of GO and GO-BODIPY in both models (Fig. 7). As shown in the monolayers (Fig. 7a), the treatment of GO in combination with light irradiation showed a negligible decrease in cell viability compared to the control. On the contrary, the treatment with GO-BODIPY showed a significant decrease in cell viability even at 50 µg/mL, confirming the results obtained in the ROS photogeneration studies. The cell viability for cells treated with 100 and 200 µg/mL was 47 and 42%, respectively. As expected, the results in spheroids confirmed the superiority of GO-BODIPY as PDT agent with a significant decrease of the cell viability to 70% compared to the control and to cells treated with similar concentration of GO (Fig. 7b). The lower PDT efficacy on the 3D model compared to the cell monolayer can be associated to the higher penetration and uptake of the material in the case of the 2D cell model leading to a higher toxicity.

A critical step in nanotechnology is the translation of "nanomaterial dose" *in vitro* to *in vivo*.[56] Traditional dose metrics are difficult to apply because of the nature of the nanomaterials, however some extrapolations can be done. The use of photodynamic therapy with dipyrromethenes in the treatment of prostate cancer has been evaluated in different clinical trials (NCT03315754, NCT01310894, NCT00305929, NCT03849365). In those trials the formulation of TOOKAD® has been assessed using doses between 2 to 4 mg/kg of bodyweight, in combination with 730 to 753 nm laser light irradiation at a power of 150 mW/cm^2 applied over 22 minutes. In our case we use a halogen white light source with a maximum in the range of 500-800 nm (centred at 732 nm) at a power of 5.4 mW/cm^2. Due to the difference in light power we decided to irradiate for a longer period of time (48 minutes), however, we believe that with the use of a more powerful light source it would be possible to reduce even more our doses and improve the ratio between the therapeutic benefit *vs* the risk of damage.

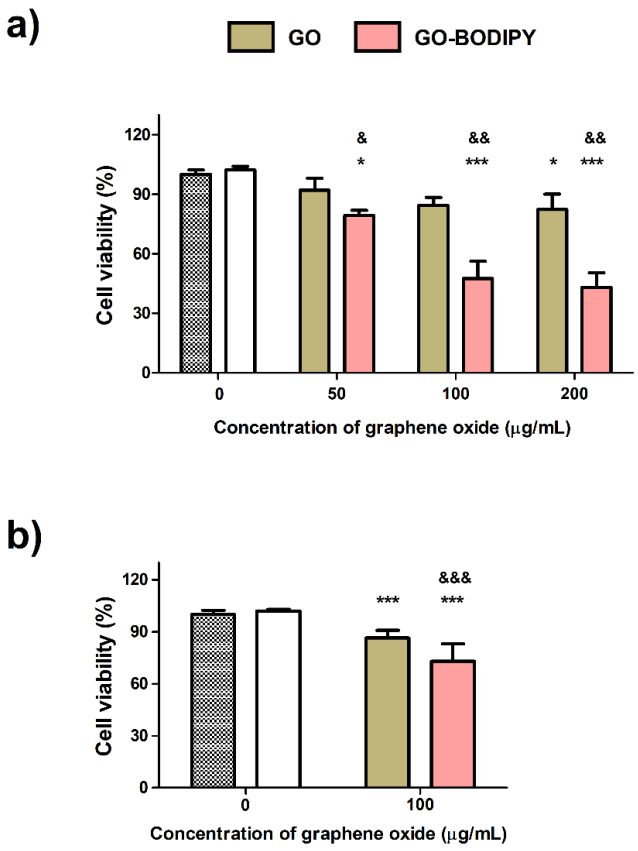

Figure 7. *In vitro* cytotoxicity of GO and GO-BODIPY combined with photoirradiation. a) PC-3 monolayers (2×10^4/well) were seeded overnight in a 96 well-plate. Then, the cells were treated with GO or GO-BODIPY at different concentrations for 24 h, then washed and irradiated with light (150×10^3 J/m^2, 48 min) (irradiated cells (solid bars), non-irradiated control (dotted bars). After the treatment, the cells were returned to the incubator for additional 24 h. The cell viability was assessed *via* the LDH assay. The results are expressed as average ± SD (n=4). Statistical analysis was performed using two-way ANOVA followed by Bonferroni post-test. * denotes comparison regarding the control (* $p<0.05$, ** $p<0.01$, *** $p<0.001$) and & denotes comparison between GO and GO-BODIPY (& $p<0.05$, && $p<0.01$). b) PC-3 spheroids (5×10^3/well) were seeded in a 1% agarose coated 96 well-plate. When the spheroids reached a size of ~600 μm (5 days after seeding), they were treated with GO or GO-BODIPY at 100 μg/mL of GO for 24 h, then washed and irradiated with light (150×10^3 J/m^2, 48 min). After the treatment, the cells were returned to the incubator for additional 24 h. Cell viability was assessed *via* the LDH assay. The results are expressed as average ± SD (n=8). Statistical analysis was performed using one-way ANOVA followed by Bonferroni post-test. * denotes comparison regarding the control (*** $p<0.001$).

Conclusions

We have demonstrated an easy and straightforward approach for covalent conjugation of BODIPY to the surface of GO *via* diol derivatisation, while preserving the BODIPY´s intrinsic properties. This strategy using a diol derivatisation reaction can be applied for a double functionalisation when combined with the epoxide ring opening, leading to the possibility to generate multifunctional adducts with targeting capability for the treatment of cancer. Furthermore, we have proved that GO-BODIPY can be used for GSH depletion and as a PDT agent *in vitro* with superior activity to GO. Our study also provides a new vision on how to apply BODIPY to treat prostate cancer. However, further work should be carried out to extend the range of applications (PDT or photothermal) of our nanomaterial in cancer therapy field.

Conflicts of interest

There are no conflicts to declare.

Acknowledgements

We gratefully acknowledge the Centre National de la Recherche Scientifique (CNRS), the International Center for Frontier Research in Chemistry (icFRC), and financial support from the Agence Nationale de la Recherche (ANR) through the LabEx project Chemistry of Complex Systems (ANR-10-LABX-0026_CSC) within the Investissement d'Avenir program (ANR-10-120 IDEX-0002-02). B.R. and G.B. thank COST action CA18103 INNOGLY: INNOvation with GLYcans: new frontiers from synthesis to new biological targets. B.R. and G.B. thank MIUR-Italy ("Progetto Dipartimenti di Eccellenza 2018-2022" allocated to Department of Chemistry "Ugo Schiff"). We would like to thank S. Guo for his help with XPS analysis, and Queen's University Belfast for funding.

References

(1) Chen, J.; Fan, T.; Xie, Z.; Zeng, Q.; Xue, P.; Zheng, T.; Chen, Y.; Luo, X.; Zhang, H. Advances in Nanomaterials for Photodynamic Therapy Applications: Status and Challenges. *Biomaterials* **2020**, *237*, 119827.

(2) Tabish, T. A.; Zhang, S.; Winyard, P. G. Developing the next Generation of Graphene-Based Platforms for Cancer Therapeutics: The Potential Role of Reactive Oxygen Species. *Redox Biol.* **2018**, *15*, 34–40.

(3) Cramer, G. M.; Moon, E. K.; Cengel, K. A.; Busch, T. M. Photodynamic Therapy and Immune Checkpoint Blockade †. *Photochem. Photobiol.* **2020**, *96*, 954–961.

(4) Zhang, W.; Ahmed, A.; Cong, H.; Wang, S.; Shen, Y.; Yu, B. Application of Multifunctional BODIPY in Photodynamic Therapy. *Dye. Pigment.* **2021**, *185*, 108937.

(5) U.S. National Library of Medicine. Clinicaltrials.gov https://clinicaltrials.gov/ct2/home.

(6) Kamkaew, A.; Lim, S. H.; Lee, H. B.; Kiew, L. V.; Chung, L. Y.; Burgess, K. BODIPY Dyes in Photodynamic Therapy. *Chem. Soc. Rev.* **2013**, *42*, 77–88.

(7) Zhao, X.; Liu, J.; Fan, J.; Chao, H.; Peng, X. Recent Progress in Photosensitizers for Overcoming the Challenges of Photodynamic Therapy: From Molecular Design to

Application. *Chem. Soc. Rev.* **2021**, *50*, 4185–4219.

(8) Marfin, Y. S.; Solomonov, A. V.; Timin, A. S.; Rumyantsev, E. V. Recent Advances of Individual BODIPY and BODIPY-Based Functional Materials in Medical Diagnostics and Treatment. *Curr. Med. Chem.* **2017**, *24*, 2745–2772.

(9) Kue, C. S.; Ng, S. Y.; Voon, S. H.; Kamkaew, A.; Chung, L. Y.; Kiew, L. V.; Lee, H. B. Recent Strategies to Improve Boron Dipyrromethene (BODIPY) for Photodynamic Cancer Therapy: An Updated Review. *Photochem. Photobiol. Sci.* **2018**, *17*, 1691–1708.

(10) Biagiotti, G.; Purić, E.; Urbančič, I.; Krišelj, A.; Weiss, M.; Mravljak, J.; Gellini, C.; Lay, L.; Chiodo, F.; Anderluh, M.; *et al.* Combining Cross-Coupling Reaction and Knoevenagel Condensation in the Synthesis of Glyco-BODIPY Probes for DC-SIGN Super-Resolution Bioimaging. *Bioorg. Chem.* **2021**, *109*, 104730.

(11) Yuan, B.; Wang, H.; Xu, J.-F.; Zhang, X. Activatable Photosensitizer for Smart Photodynamic Therapy Triggered by Reactive Oxygen Species in Tumor Cells. *ACS Appl. Mater. Interfaces* **2020**, *12*, 26982–26990.

(12) Liu, M.; Li, C. Recent Advances in Activatable Organic Photosensitizers for Specific Photodynamic Therapy. *Chempluschem* **2020**, *85*, 948–957.

(13) Zhou, Y.; Wong, R. C. H.; Dai, G.; Ng, D. K. P. A Bioorthogonally Activatable Photosensitiser for Site-Specific Photodynamic Therapy. *Chem. Commun.* **2020**, *56*, 1078–1081.

(14) Durantini, A. M.; Greene, L. E.; Lincoln, R.; Martínez, S. R.; Cosa, G. Reactive Oxygen Species Mediated Activation of a Dormant Singlet Oxygen Photosensitizer: From Autocatalytic Singlet Oxygen Amplification to Chemicontrolled Photodynamic Therapy. *J. Am. Chem. Soc.* **2016**, *138*, 1215–1225.

(15) Zhang, J.; Wang, N.; Ji, X.; Tao, Y.; Wang, J.; Zhao, W. BODIPY-Based Fluorescent Probes for Biothiols. *Chem. – A Eur. J.* **2020**, *26*, 4172–4192.

(16) Giacomazzo, G. E.; Palladino, P.; Gellini, C.; Salerno, G.; Baldoneschi, V.; Feis, A.; Scarano, S.; Minunni, M.; Richichi, B. A Straightforward Synthesis of Phenyl Boronic Acid (PBA) Containing BODIPY Dyes: New Functional and Modular Fluorescent Tools for the Tethering of the Glycan Domain of Antibodies. *RSC Adv.* **2019**, *9*, 30773–30777.

(17) Cheng, X.; Xu, H.-D.; Ran, H.-H.; Liang, G.; Wu, F.-G. Glutathione-Depleting Nanomedicines for Synergistic Cancer Therapy. *ACS Nano* **2021**, *15*, 8039–8068.

(18) Karki, N.; Tiwari, H.; Tewari, C.; Rana, A.; Pandey, N.; Basak, S.; Sahoo, N. G. Functionalized Graphene Oxide as a Vehicle for Targeted Drug Delivery and Bioimaging Applications. *J. Mater. Chem. B* **2020**, *8*, 8116–8148.

(19) Reina, G.; Ruiz, A.; Murera, D.; Nishina, Y.; Bianco, A. "Ultramixing": A Simple and Effective Method To Obtain Controlled and Stable Dispersions of Graphene Oxide in Cell Culture Media. *ACS Appl. Mater. Interfaces* **2019**, *11*, 7695–7702.

(20) Liu, J.; Cui, L.; Losic, D. Graphene and Graphene Oxide as New Nanocarriers for Drug Delivery Applications. *Acta Biomater.* **2013**, *9*, 9243–9257.

(21) Newman, L.; Rodrigues, A. F.; Jasim, D. A.; Vacchi, I. A.; Ménard-Moyon, C.; Bianco, A.; Bussy, C.; Kostarelos, K. Nose-to-Brain Translocation and Cerebral Biodegradation of Thin Graphene Oxide Nanosheets. *Cell Reports Phys. Sci.* **2020**, *1*, 100176.

(22) Sharker, S. M.; Jeong, C. J.; Kim, S. M.; Lee, J.-E.; Jeong, J. H.; In, I.; Lee, H.; Park, S. Y. Photo- and PH-Tunable Multicolor Fluorescent Nanoparticle-Based Spiropyran- and BODIPY-Conjugated Polymer with Graphene Oxide. *Chem. - An Asian J.* **2014**, *9*, 2921–2927.

(23) Lee, S. Y.; Kim, S. H.; Kim, S. M.; Lee, H.; Lee, G.; Park, S. Y. Tunable and Selective Detection of Cancer Cells Using a Betainized Zwitterionic Polymer with BODIPY and Graphene Oxide. *New J. Chem.* **2014**, *38*, 2225–2228.

(24) Xu, X.-L.; Shao, J.; Chen, Q.-Y.; Li, C.-H.; Kong, M.-Y.; Fang, F.; Ji, L.; Boison, D.; Huang, T.; Gao, J.; *et al.* A Mn(II) Complex of Boradiazaindacene (BODIPY) Loaded Graphene Oxide as Both LED Light and H2O2 Enhanced Anticancer Agent. *J. Inorg. Biochem.* **2016**, *159*, 1–6.

(25) LORAND, J. P.; EDWARDS, J. O. Polyol Complexes and Structure of the Benzeneboronate Ion. *J. Org. Chem.* **1959**, *24*, 769–774.

(26) Stubelius, A.; Lee, S.; Almutairi, A. The Chemistry of Boronic Acids in Nanomaterials for Drug Delivery. *Acc. Chem. Res.* **2019**, *52*, 3108–3119.

(27) Burress, J. W.; Gadipelli, S.; Ford, J.; Simmons, J. M.; Zhou, W.; Yildirim, T. Graphene Oxide Framework Materials: Theoretical Predictions and Experimental Results. *Angew. Chemie Int. Ed.* **2010**, *49*, 8902–8904.

(28) He, D.; He, X.; Wang, K.; Zou, Z.; Yang, X.; Li, X. Remote-Controlled Drug Release from Graphene Oxide-Capped Mesoporous Silica to Cancer Cells by Photoinduced PH-

Jump Activation. *Langmuir* **2014**, *30*, 7182–7189.

(29) Morimoto, N.; Kubo, T.; Nishina, Y. Tailoring the Oxygen Content of Graphite and Reduced Graphene Oxide for Specific Applications. *Sci. Rep.* **2016**, *6*, 21715.

(30) Chau, N. D. Q.; Reina, G.; Raya, J.; Vacchi, I. A.; Ménard-Moyon, C.; Nishina, Y.; Bianco, A. Elucidation of SiRNA Complexation Efficiency by Graphene Oxide and Reduced Graphene Oxide. *Carbon N. Y.* **2017**, *122*, 643–652.

(31) Shard, A. G. Detection Limits in XPS for More than 6000 Binary Systems Using Al and Mg Kα X-Rays. *Surf. Interface Anal.* **2014**, *46*, 175–185.

(32) Wepasnick, K. A.; Smith, B. A.; Bitter, J. L.; Howard Fairbrother, D. Chemical and Structural Characterization of Carbon Nanotube Surfaces. *Anal. Bioanal. Chem.* **2010**, *396*, 1003–1014.

(33) Guo, S.; Nishina, Y.; Bianco, A.; Ménard-Moyon, C. A Flexible Method for Covalent Double Functionalization of Graphene Oxide. *Angew. Chemie Int. Ed.* **2020**, *59*, 1542–1547.

(34) Vacchi, I. A.; Raya, J.; Bianco, A.; Ménard-Moyon, C. Controlled Derivatization of Hydroxyl Groups of Graphene Oxide in Mild Conditions. *2D Mater.* **2018**, *5*, 035037.

(35) Zlatić, K.; Ayouchia, H. B. El; Anane, H.; Mihaljević, B.; Basarić, N.; Rohand, T. Spectroscopic and Photophysical Properties of Mono- and Dithiosubstituted BODIPY Dyes. *J. Photochem. Photobiol. A Chem.* **2020**, *388*, 112206.

(36) Yang, Y.; Liu, T. Fabrication and Characterization of Graphene Oxide/Zinc Oxide Nanorods Hybrid. *Appl. Surf. Sci.* **2011**, *257*, 8950–8954.

(37) Karousis, N.; Sandanayaka, A. S. D.; Hasobe, T.; Economopoulos, S. P.; Sarantopoulou, E.; Tagmatarchis, N. Graphene Oxide with Covalently Linked Porphyrin Antennae: Synthesis, Characterization and Photophysical Properties. *J. Mater. Chem.* **2011**, *21*, 109–117.

(38) Du, Y.; Dong, N.; Zhang, M.; Zhu, K.; Na, R.; Zhang, S.; Sun, N.; Wang, G.; Wang, J. Covalent Functionalization of Graphene Oxide with Porphyrin and Porphyrin Incorporated Polymers for Optical Limiting. *Phys. Chem. Chem. Phys.* **2017**, *19*, 2252–2260.

(39) Andreozzi, P.; Tamberi, L.; Tasca, E.; Giacomazzo, G. E.; Martinez, M.; Severi, M.; Marradi, M.; Cicchi, S.; Moya, S.; Biagiotti, G.; *et al.* The B & B Approach: Ball-Milling

Conjugation of Dextran with Phenylboronic Acid (PBA)-Functionalized BODIPY. *Beilstein J. Org. Chem.* **2020**, *16*, 2272–2281.

(40) Garg, K.; Shanmugam, R.; Ramamurthy, P. C. New Covalent Hybrids of Graphene Oxide with Core Modified and -Expanded Porphyrins: Synthesis, Characterisation and Their Non Linear Optical Properties. *Carbon N. Y.* **2017**, *122*, 307–318.

(41) Sun, S.; Zhuang, X.; Wang, L.; Liu, B.; Zhang, B.; Chen, Y. BODIPY-Based Conjugated Polymer Covalently Grafted Reduced Graphene Oxide for Flexible Nonvolatile Memory Devices. *Carbon N. Y.* **2017**, *116*, 713–721.

(42) Niu, L.-Y.; Guan, Y.-S.; Chen, Y.-Z.; Wu, L.-Z.; Tung, C.-H.; Yang, Q.-Z. BODIPY-Based Ratiometric Fluorescent Sensor for Highly Selective Detection of Glutathione over Cysteine and Homocysteine. *J. Am. Chem. Soc.* **2012**, *134*, 18928–18931.

(43) Ortega, A. L.; Mena, S.; Estrela, J. M. Glutathione in Cancer Cell Death. *Cancers (Basel).* **2011**, *3*, 1285–1310.

(44) Townsend, D. M.; Tew, K. D. The Role of Glutathione-S-Transferase in Anti-Cancer Drug Resistance. *Oncogene* **2003**, *22*, 7369–7375.

(45) Landi, S. Mammalian Class Theta GST and Differential Susceptibility to Carcinogens: A Review. *Mutat. Res. Mutat. Res.* **2000**, *463*, 247–283.

(46) Raza, H. Dual Localization of Glutathione S-Transferase in the Cytosol and Mitochondria: Implications in Oxidative Stress, Toxicity and Disease. *FEBS J.* **2011**, *278*, 4243–4251.

(47) Dixon, D. P.; Hawkins, T.; Hussey, P. J.; Edwards, R. Enzyme Activities and Subcellular Localization of Members of the Arabidopsis Glutathione Transferase Superfamily. *J. Exp. Bot.* **2009**, *60*, 1207–1218.

(48) Wang, X.; Li, S.; Liu, Y.; Ma, C. Redox Regulated Peroxisome Homeostasis. *Redox Biol.* **2015**, *4*, 104–108.

(49) Pinto, A. M.; Gonçalves, I. C.; Magalhães, F. D. Graphene-Based Materials Biocompatibility: A Review. *Colloids Surfaces B Biointerfaces* **2013**, *111*, 188–202.

(50) Askari, E.; Naghib, S. M.; Seyfoori, A.; Maleki, A.; Rahmanian, M. Ultrasonic-Assisted Synthesis and in Vitro Biological Assessments of a Novel Herceptin-Stabilized Graphene Using Three Dimensional Cell Spheroid. *Ultrason. Sonochem.* **2019**, *58*, 104615.

(51) Pelin, M.; Fusco, L.; Martín, C.; Sosa, S.; Frontiñán-Rubio, J.; González-Domínguez, J. M.; Durán-Prado, M.; Vázquez, E.; Prato, M.; Tubaro, A. Graphene and Graphene Oxide

Induce ROS Production in Human HaCaT Skin Keratinocytes: The Role of Xanthine Oxidase and NADH Dehydrogenase. *Nanoscale* **2018**, *10*, 11820–11830.

(52) Eruslanov, E.; Kusmartsev, S. Identification of ROS Using Oxidized DCFDA and Flow-Cytometry. In *Methods in molecular biology (Clifton, N.J.)*; United States, United States, 2010; Vol. 594, pp. 57–72.

(53) Lammel, T.; Boisseaux, P.; Fernández-Cruz, M.-L.; Navas, J. M. Internalization and Cytotoxicity of Graphene Oxide and Carboxyl Graphene Nanoplatelets in the Human Hepatocellular Carcinoma Cell Line Hep G2. *Part. Fibre Toxicol.* **2013**, *10*, 27.

(54) Prieto-Montero, R.; Prieto-Castañeda, A.; Sola-Llano, R.; Agarrabeitia, A. R.; García-Fresnadillo, D.; López-Arbeloa, I.; Villanueva, A.; Ortiz, M. J.; Moya, S.; Martínez-Martínez, V. Exploring BODIPY Derivatives as Singlet Oxygen Photosensitizers for PDT. *Photochem. Photobiol.* **2020**, *96*, 458–477.

(55) Riss, T.; Trask, O. J. Factors to Consider When Interrogating 3D Culture Models with Plate Readers or Automated Microscopes. *Vitr. Cell. Dev. Biol. - Anim.* **2021**, *57*, 238–256.

(56) Elsaesser, A.; Howard, C. V. Toxicology of Nanoparticles. *Adv. Drug Deliv. Rev.* **2012**, *64*, 129–137.